Topological mixed valence model in magic-angle twisted bilayer graphene

Yantao Li, Benjamin M. Fregoso, and Maxim Dzero
Department of Physics, Kent State University, Kent, Ohio 44242, USA

(Received 2 October 2023; revised 26 April 2024; accepted 24 June 2024; published 12 July 2024)

We develop a model to describe the mixed valence regime in magic-angle twisted bilayer graphene (MATBG) using the recently developed heavy-fermion framework. By employing the large-N slave-boson approach, we derive the self-consistent mean-field equations and solve them numerically. We find that the SU(8) local flat-band electron symmetry constraint moiré system exhibits mixed valence properties that are different from conventional heavy-fermion systems. We find the solutions describing the physics at the filling near the Mott insulator regime in the limit of strong Coulomb interactions between the flat-band fermions. Our model can provide additional insight into the possible microscopic origin of unconventional superconductivity in MATBG.

DOI: 10.1103/PhysRevB.110.045123

I. INTRODUCTION

The discovery of correlated electronic phases including superconductivity in magic-angle twisted bilayer graphene (MATBG) [1,2] has stimulated research efforts to explore various electronic properties in graphene-based multilayer structures [3–11] as well as in van der Waals heterostructures and other platforms [12–19]. As a result, a new field referred to as "twistronic physics" has emerged [20], which focuses on the theoretical aspects of these systems and covers both static [21–40] and nonequilibrium properties [41–45].

The MATBG system consists of two single graphene sheets that are twisted relative to each other at certain angles called magic angles [46–52]. It is believed that it is the flat bands that appear at such magic angles that are the main driver for the exotic physical phenomena which were experimentally observed in these systems. The origin of magic angles is related to the case when the electron tunneling in the AA region of MATBG is neglected corresponding to the chiral limit [53,54]. It can be theoretically shown that one does not need to use the chiral limit for other twisted graphene stacks to exhibit such flat bands associated with Dirac cones [55]. Furthermore, the discovery of superconductivity in MATBG demonstrates yet another example of superconductivity emerging from the "strange metal" phase [56] and, as such, is reminiscent of the physics of the high-T_c copper-based and heavy-fermion superconductors. In passing, we note that several works have recently attempted to explain the origin of superconductivity in MATBG from various perspectives [57–61].

The MATBG can also be seen as localized states coupled with Dirac fermions in the early studies [62–64]. Most recently an alternative viewpoint has emerged. Specifically, focusing on a first magic angle, Song and Bernevig showed that a model for twisted bilayer graphene can be mapped to the topological heavy-fermion model [65]. This elegant theory is based on the experimental fact that the AA region in MATBG exhibits a quantum-dot-like behavior [66–68] and so one can describe the physics of this region using a model with the flat-band electrons (f electrons). The electrons in the AB/BA regions play the role of topological conduction electrons (c electrons). By mapping the Bistritzer-MacDonald (BM) model [46] to the periodic Anderson model at the first magic angle, Song and Bernevig created a way to bridge the MATBG with the more conventional heavy-fermion systems. Hence, the topological flat bands of the BM model can be seen as a result of the hybridization of f electrons and topological c electrons. However, in striking contrast with the conventional heavy-fermion system, the MATBG hosts SU(8) symmetry due to spin and valley degrees of freedom and two central flat bands. Shortly after, several important works appeared, which addressed various aspects of this unique moiré heavy-fermion-like system [69–79].

The heavy-fermion picture provides a potential direct way to explain various experiment signatures in the MATBG, such as the cascade of electronic transitions [67], the Pomeranchuk effect [80,81], Hubbard-band-like features in scanning tunneling microscopy (STM) [66], and a sawtoothlike feature of inverse compressibility [82]. Previous theoretical works on the heavy-fermion picture of MATBG tried to explain the above experimental results [69–79]. Especially, a unified theory of such a heavy-fermion picture including the dynamical mean-field theory (DMFT) can predict the Kondo temperature at all of the fillings and temperature-dependent behaviors [74]. Another DMFT work presents the temperature dependence of various properties in MATBG [75].

In conventional heavy-fermion systems, one usually distinguishes between the so-called local moment (or Kondo) regime and the mixed valent one. In the local moment regime, the energy of the flat (f-orbital) band lies well below the Fermi energy of the conduction electrons, while in the mixed valent regime, it lies close to the Fermi energy. In order to describe both of these regimes on a technical level, one considers the limit when the local Coulomb repulsion is taken to infinity. Then one introduces the projection operators along with the Lagrange multiplier to enforce the constraint of the single occupancy on the f levels. In the mean-field approximation, one replaces the projection operators and constraint fields with the c numbers which are computed self-consistently and describe the renormalization of the f-energy level, hybridization

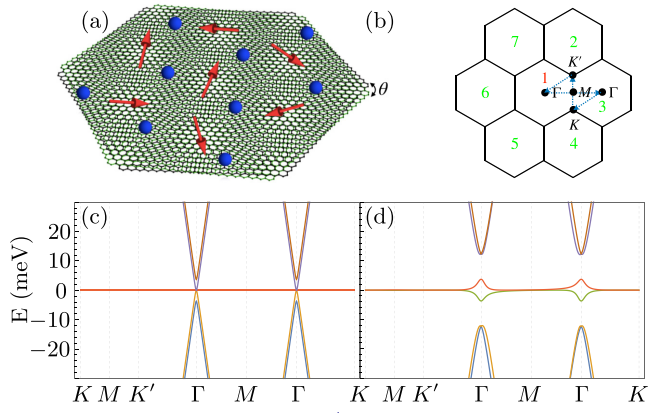

FIG. 1. (a) Sketch of the setup. Two single graphene layers twist relative to each other with angle $\theta = \theta_m$. The AA regions behave as quantum dots (red arrows) and AB/BA regions behave as conduction states (blue spheres). (b) Moiré momentum space with seven mBZs. The blue dashed lines mean the path of the spectrum. (c) and (d) are the spectrum of valley $\eta = +$ with parameters $\bar{\rho} = 0$ (before hybridization) and $\bar{\rho} = 0.5$ (full hybridization) separately. Also, both of them are set with $\mu_f = \bar{\lambda} = 0$ and other parameters can be seen in the main text. Note that $\mu_f = \bar{\lambda} = 0$ is not the solution of the mean-field equations.

between c and f electrons, as well as renormalization of the chemical potential.

Early works on the application of the heavy-fermion model to MATBG have typically focused on the Kondo regime and have not solved the problem self-consistently in the mixed valence regime based on the mean-field equations. In this paper, we attempt to resolve this issue. In what follows, we present a different heavy-fermion model for the MATBG and discuss the physics both in the Kondo regime and the mixed valence regime self-consistently with the infinite f-electron Coulomb interaction. Our self-consistent solutions pave the way to go beyond the mean-field approximation and consider the effects of fluctuations on the competing phases of MATBG. However, it should be noted that different from the previous DMFT method [74,75], our model provides an analytic way to understand the temperature-dependent behaviors in MATBG.

An important aspect of our model is that we consider the strong limit of Coulomb interactions, which could provide another way to explain the microscopic origin of unconventional (d-wave) superconductivity, and can be shown to arise from the quantum mechanical fluctuations in the number of the f electrons and is purely electronic in origin. Indeed, as the very recent experiment suggests [83], the MATBG does indicate the d-wave superconductivity similar to the Cooper pair symmetry of the superconductivity in the conventional heavy-fermion systems [84].

II. SETUP AND TOPOLOGICAL HEAVY-FERMION MODEL

The MATBG setup is illustrated in Fig. 1(a). Two single graphene layers are stacked together and they are twisted relative to each other with angle θ. The AA regions are designated by white spots (with red arrows depicting flat-band electrons) and AB/BA regions are dark green (with blue spheres depicting conduction electrons).

Next, we consider the first magic angle $\theta_m = 1.05^\circ$. At this magic angle, the MATBG can be mapped from the Bistritzer-MacDonald model to a special SU(8) periodic Anderson model, i.e., the Song-Bernevig model (SB) [65]. We choose the SB model as the starting point. The Hamiltonian is

$$\hat{H} = \hat{H}_{0,\mathrm{c}} + \hat{H}_{0,\mathrm{f}} + \hat{H}_{0,\mathrm{cf}} + \hat{H}_{\mathrm{U}}, \tag{1}$$

where

$$\hat{H}_{0\mathrm{c}} = \sum_{a,a',\eta,s} \sum_{\mathbf{p}} h^{(c,\eta s)}_{aa'}(\mathbf{p}) c^{\dagger}_{\mathbf{p},a,\eta,s} c_{\mathbf{p},a',\eta,s} \tag{2}$$

is the Hamiltonian of the conduction (c) electrons in AB/BA moiré lattice sites,

$$\hat{H}_{0\mathrm{f}} = \sum_{\alpha,\alpha',\eta,s} \sum_{\mathbf{k}} h^{(f,\eta s)}_{\alpha\alpha'}(\mathbf{k}) f^{\dagger}_{\mathbf{k},\alpha,\eta,s} f_{\mathbf{k},\alpha',\eta,s} \tag{3}$$

is the Hamiltonian of flat-band (f) electrons in AA moiré lattice sites,

$$\hat{H}_{0\mathrm{cf}} = \sum_{\alpha,a,\eta,s} \sum_{\mathbf{G}} \sum_{\mathbf{k}\in \mathrm{mBZ}} \left[V^{(\eta s)}_{\alpha a}(\mathbf{k}+\mathbf{G}) f^{\dagger}_{\mathbf{k},\alpha,\eta,s} c_{\mathbf{k}+\mathbf{G},a,\eta,s} + \mathrm{H.c.} \right], \tag{4}$$

accounts for the hybridization between the c and f electrons, and

$$\hat{H}_{\mathrm{U}} = \frac{U}{2} \sum_{\mathbf{R}} : \hat{n}^f_{\mathbf{R}} :: \hat{n}^f_{\mathbf{R}} : \tag{5}$$

is the Hamiltonian describing the local Coulomb repulsion between the f electrons. In the expressions above $\alpha = 1, 2$, $a = 1, 2, 3, 4$, $\eta = \pm$, and $s = \uparrow, \downarrow$ are the flat band, conduction band, valley, and spin indices correspondingly, $\mathbf{p} = \mathbf{k} + \mathbf{G}$, $\mathbf{G}$ is the reciprocal lattice vectors in the moiré momentum space, $\hat{n}^f_{\mathbf{R}}$ is the on-site density operator of f electrons, and U is the strength of the Coulomb repulsion. Note that we did not consider the interactions between the c electrons and also ignore the interactions between c and f electrons. Lastly, the matrices that appear in the expressions above are defined according to

$$\hat{h}^{(c,\eta s)}(\mathbf{p}) = \begin{bmatrix} -\mu_c \hat{\sigma}_0 & v_\star(\eta p_x \hat{\sigma}_0 + i p_y \hat{\sigma}_z) \\ v_\star(\eta p_x \hat{\sigma}_0 - i p_y \hat{\sigma}_z) & M\hat{\sigma}_x - \mu_c \hat{\sigma}_0 \end{bmatrix},$$
$$V^{(\eta s)}(\mathbf{p}) = e^{\frac{-|\mathbf{p}|^2\lambda_d^2}{2}} \begin{bmatrix} \gamma \hat{\sigma}_0 + v'_\star(\eta p_x \hat{\sigma}_x + p_y \hat{\sigma}_y) \\ 0_{2\times 2} \end{bmatrix}, \tag{6}$$

and $h^{(f,\eta s)} = (\epsilon_{f_0} - \mu_f)\hat{\sigma}_0$, where ϵ_{f_0} is the initial energy level of f electrons, μ_c and μ_f are the chemical potentials for c and f electrons accordingly, $\hat{\sigma}_0 = I_{2\times 2}$ is the unit matrix, and $\hat{\sigma}_j$ ($j = x, y, z$) are the Pauli matrices. Note that the Hamiltonian is expressed in the moiré momentum space using the plane-wave approximation. The size of the moiré momentum space (per valley per spin) is $2 + 4N_G$ which means two flat bands and four conduction bands with N_G moiré Brillouin zones (mBZs). The values of the parameters are $v_\star = -4.303$ eV Å, $M = 3.697$ meV, $\gamma = -24.75$ meV, $v'_\star = 1.622$ eV Å, and the damping factor $\lambda_d = 0.3375 a_M$, where a_M is the moiré lattice constant. Note that all these parameters correspond to the "magic angle" $\theta_m = 1.05^\circ$, $U_0 = W_{AA}/W_{AB} = 0.8$, W_{AA}

and W_{AB} are interlayer hopping amplitudes in AA regions, and AB/BA regions separately, and the velocity of the electron in single-layer graphene $v_F = 5.94$ eV Å. We note that when $M = 0$ the system reaches the limit of the flat band and we do *not* consider this case in this paper.

III. SLAVE-BOSON APPROACH AND MEAN-FIELD EQUATIONS

To handle the SB model in the mixed valence region, we use the slave-boson approach. We extend the number of orbital, spin, and valley for both c and f electrons to N flavors and set the interaction

$$U = \infty \tag{7}$$

to exclude the double occupancy. Introducing the slave-boson operators $b^\dagger_{\mathbf{R}}$ and $b_{\mathbf{R}}$ at each AA site in real space, the constraint becomes

$$Q = \sum_{l=1}^{N}\sum_{\alpha}(f^\dagger_{\mathbf{R},\alpha,l} f_{\mathbf{R},\alpha,l} + b^\dagger_{\mathbf{R}} b_{\mathbf{R}}). \tag{8}$$

Note that $N = 4$ includes spin and valley for two flat-band orbitals. Since f electrons do not depend on the valley, we choose c-electron bands of the valley $\eta = +$ in the above Hamiltonian. We stress that there are two index spaces in the Hamiltonian. One is the extended N space with $1/N$ expansion corresponding to the index l. Another is the moiré momentum space which has a size of $2 + 4N_G$ corresponding to the index α, α', a, and a' separately. We introduce Lagrangian multipliers $\lambda_{\mathbf{R}}$ to ensure the number of f electrons is $Q = 1$. We rewrite $Q \to q_0 N$, $b_{\mathbf{R}} \to b_{\mathbf{R}}\sqrt{N}$, and $V_{\alpha a} \to V_{\alpha a}/\sqrt{N}$. The local gauge transformation is $b_{\mathbf{R}} = \rho_{\mathbf{R}} \exp(i\theta_{\mathbf{R}})$, $f_{\mathbf{R}} = f'_{\mathbf{R}} \exp(i\theta_{\mathbf{R}})$, and $\lambda_{\mathbf{R}} = \lambda'_{\mathbf{R}} - \theta_{\mathbf{R}}$. We then rewrite $f'_{\mathbf{R}}$ and $\lambda'_{\mathbf{R}}$ to $f_{\mathbf{R}}$ and $\lambda_{\mathbf{R}}$. The partition function is

$$Z = \int \mathscr{D}(cc^\dagger f f^\dagger \rho\lambda)\exp(-S), \tag{9}$$

where the action is $S = \int_0^\beta L(\tau)d\tau$, and

$$\begin{aligned} L = &\sum_{\substack{a,a';l=1\\ \mathbf{p}}}^{N}\left[\partial_\tau + h^{(c)}_{aa'}(\mathbf{p})\right]c^\dagger_{\mathbf{p},a,l}c_{\mathbf{p},a',l}(\tau) + \sum_{\substack{\alpha,\alpha'\\ \mathbf{k},\mathbf{k}'\in\mathrm{mBZ}}}\left(\partial_\tau + h^{(f)}_{\alpha\alpha'}(\mathbf{k})\delta_{\mathbf{k},\mathbf{k}'} + \frac{i\lambda(\mathbf{k}-\mathbf{k}';\tau)}{\sqrt{N_L}}\right)f^\dagger_{\mathbf{k},\alpha,l}f_{\mathbf{k}',\alpha',l}(\tau) \\ &+ \frac{1}{\sqrt{N_L}}\sum_{\substack{\mathbf{G},\alpha,a;l=1\\ \mathbf{k},\mathbf{k}'\in\mathrm{mBZ}}}^{N}\left[V_{\alpha a}(\mathbf{k}+\mathbf{G})c^\dagger_{\mathbf{k}+\mathbf{G},a,l}(\tau)f_{\mathbf{k}',\alpha,l}(\tau)\rho^\dagger(\mathbf{k}-\mathbf{k}';\tau) + \mathrm{H.c.}\right] \\ &+ \frac{iN}{\sqrt{N_L}}\sum_{\mathbf{k},\mathbf{k}'\in\mathrm{mBZ}}\rho(\mathbf{k};\tau)\lambda(\mathbf{k}'-\mathbf{k};\tau)\rho(-\mathbf{k}';\tau) - iq_0N\sqrt{N_L}\lambda(0;\tau), \end{aligned} \tag{10}$$

where c, $c^\dagger$, f, and $f^\dagger$ are the creation and annihilation operators for c and f electrons separately, τ is the time, $\beta = \frac{1}{T}$, T is the temperature, and N_L is the number of lattice sites in moiré real space. We set $\lambda(\mathbf{k};\tau) = \frac{1}{T}\bar{\lambda}\delta_{\mathbf{k},0}$, $\rho(\mathbf{k};\tau) = \frac{1}{T}\bar{\rho}\delta_{\mathbf{k},0}$ to get the mean-field action. We rewrite $\frac{\bar{\lambda}}{\sqrt{N_L}} \to \bar{\lambda}$ and $\frac{\bar{\rho}}{\sqrt{N_L}} \to \bar{\rho}$. After applying $\partial S_0/\partial\bar{\rho} = 0$, $\partial S_0/\partial\bar{\lambda} = 0$, and summing over the Matsubara frequency ω_n, we end up with three mean-field equations as follows,

$$\bar{\rho}\bar{\lambda} = \frac{i}{2N_L}\sum_{\mathbf{k}\in\mathrm{mBZ}}\sum_{j}^{2+4N_G}\left(P^\dagger A_0^{\bar{\rho}}P\right)_{jj}\cdot n_F(\mathcal{E}_j), \tag{11}$$

$$q_0 - \bar{\rho}^2 = -\frac{i}{N_L}\sum_{\mathbf{k}\in\mathrm{mBZ}}\sum_{j}^{2+4N_G}(P^\dagger A_0^{\bar{\lambda}}P)_{jj}\cdot n_F(\mathcal{E}_j), \tag{12}$$

$$n_t = q_0 - \bar{\rho}^2 + \frac{1}{N_L}\sum_{\mathbf{k}\in\mathrm{mBZ}}\sum_{j}^{2+4N_G}\left(P^\dagger A_0^{c}P\right)_{jj}\cdot n_F(\mathcal{E}_j) - 2N_G, \tag{13}$$

where $\bar{\rho}$ is the slave boson and $\bar{\lambda}$ is the Lagrangian multiplier at the saddle points accordingly, n_t is the total filling, $n_F(\epsilon) = [\exp(\epsilon/T) + 1]^{-1}$ is the Fermi-Dirac distribution, $\mathcal{E}_j$ is the eigenvalues of matrix $A_0 = \{\{\hat{h}^{(c)}, \hat{V}\}, \{\hat{V}^\dagger, \hat{h}^{(f)} + i\bar{\lambda}\hat{\sigma}_0\}\}$, $A_0^{\bar{\rho}} = \partial(-i\omega_n + A_0)/\partial\bar{\rho}$, $A_0^{\bar{\lambda}} = \partial(-i\omega_n + A_0)/\partial\bar{\lambda}$, $A_0^{c} = -\partial(-i\omega_n + A_0)/\partial\mu_c$, and A_0 expands in the moiré momentum space. Note that P can be constructed by the eigenvectors of A_0 and $P = (c_1, c_2, \ldots, c_{(2+4N_G)})_{2+4N_G\times 2+4N_G}$, where c_j are the eigenvectors of A_0. (See Supplemental Material [85].) The above three self-consistent mean-field equations are one of our main results.

IV. NUMERICS

Now, we will numerically solve Eqs. (11)–(13). To solve them self-consistently, we set an error bar errs $= \sum_{n=1}^{3}(l_n - r_n)^2$, where l_n and r_n represent the left- and right-hand sides of nth mean-field equation separately. We set $\epsilon_{f_0} = 0$, $\mu_c = \mu_f$, and go through the parameter regions $\bar{\rho} \in [0, 0.5]$, $\mu_f \in [-100, 100]$ meV, and $i\bar{\lambda} \in [-100, 100]$ meV. Since we set the interaction $U = \infty$, $Q = 1$, so we have $q_0 = 1/4$. To reach the mixed valence regime, we also set the total filling $n_t = 0.8q_0$. We find the solutions to make the errs $\approx$0. There exist two solutions: One is positive μ_f, and another is negative μ_f as shown in Figs. 2(a) and 2(b). We note that $\mathcal{E}_j(\bar{\lambda}, \bar{\rho}, \mu_f, \mathbf{k})$ is numerically calculated and depends on the chemical potential μ_f and momentum $\mathbf{k}$ with $\mathbf{k} \in$ mBZ.

We substitute the solutions to A_0 and we get the spectra (see Fig. 2). We also plot the variation of parameters in the

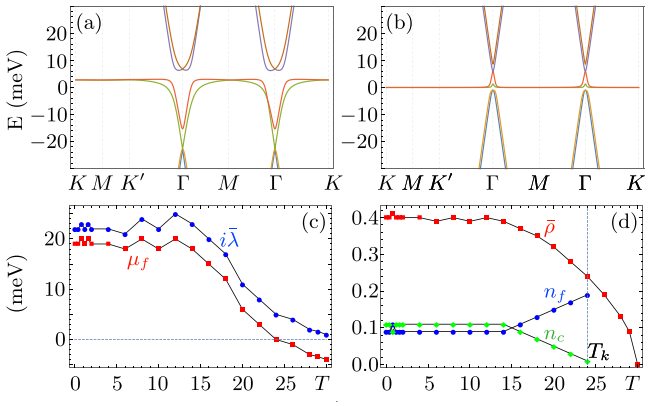

FIG. 2. (a) Spectrum of the self-consistent solutions for valley $\eta = +$ with parameters $\mu_f = 19$ meV, $i\bar{\lambda} = 22$ meV, $\bar{\rho} = 0.4$, and $T = 0.01$ K. (b) The spectrum of the self-consistent solutions with parameters $\mu_f = -5$ meV, $i\bar{\lambda} = -5$ meV, $\bar{\rho} = 0.1$, and $T = 0.01$ K. (c) Self-consistent solutions μ_f and $i\bar{\lambda}$ vs T. (d) Self-consistent solutions ρ, n_f, and n_c vs T with $n_t = 0.8q_0$, where $T_k \approx 24$ K is the Kondo temperature.

mixed valence region as a function of the temperature T (see Fig. 2). We estimate the Kondo temperature $T_k \approx 24$ K.

V. DISCUSSION

As shown in Fig. 2(d), the topological mixed valence model in MATBG undergoes a unique linear continuous transition from the Kondo regime to the mixed valence regime from the temperature $T = T_K \approx 24$ K to $T \approx 16$ K. This is in sharp difference with conventional heavy-fermion materials which undergo a first-order transition [86,87] or a nonlinear continuous transition [88]. The reason behind this is the dispersion of the topological conduction electrons (linear dispersion at higher energies and parabolic dispersion at lower energies) in the AB regions of MATBG. As the chemical potential μ_f is leveling up to positive values as the temperature decreases [see Fig. 2(c)], the flat bands (valence bands) immediately interact with the conduction bands. This unique linear decrease of n_f (or linear increase of n_c) reflects the linear dispersion of the topological conduction electrons at high energies. Thus our self-consistent calculation at finite temperature predicts the linear-in-T behavior of the concentration of the f electrons. This unique temperature dependence of n_f may be experimentally tested by x-ray emission spectroscopy [88,89], which could further confirm that MATBG is a heavy-fermion material.

As the increasing temperature in MATBG, one could explain the Pomeranchuk effect [80,81] where a local moment develops upon heating. Our results can also give insight into the heating process from the mixed valence regime to the Kondo regime. Since the condensation of slave boson in the AA region, the local moment in the AA region is formed in terms of n_f as the temperature increases to the Kondo temperature. The temperature dependence behavior we obtained can also be used to predict the possible superconductivity transition temperature. The valence fluctuations can induce d-wave superconductivity as suggested in conventional heavy-fermion materials [90,91]. Further detailed calculations of the transition temperature of superconductivity based on our model will be the subject of future work.

Different from the conventional heavy-fermion system, the topological mixed valence model in MATBG has SU(8) symmetry for local moments (spin, valley, band) in the regime of $M \ll \gamma \ll U$. The two central flat bands for each valley and spin are particle-hole symmetric in the chiral limit. Although the particle-hole symmetry is broken at the experimental lattice relaxation range $U_0 = 0.8$, the valence bands host a similar band structure as the conduction bands before the hybridization. This makes it difficult to reach the Kondo regime just by pushing the flat bands lower, away from the conduction bands as it does in the conventional heavy-fermion system. One needs to consider many valence bands together.

VI. SUMMARY

We have introduced a model to describe the mixed valence regime of the magic-angle twisted bilayer graphene with an infinite Coulomb interaction. We start from the SB model and use the slave-boson method in a large-N expansion. We derive a group of mean-field equations to describe the mixed valence regime of twisted bilayer graphene. The solutions can catch the physics of the filling near the strong correlation, which is at the edge of the Mott insulator, and then could be approaching the unconventional superconductivity. Our topological mixed valence model paves the way to study the possible origin of superconductivity in twisted bilayer graphene. We hope our model could stimulate further research in the mixed valence regime in various related van der Waals heterostructures materials or platforms.

Note added. Recently, we became aware of Ref. [92], which deals with the mixed valence model in twisted bilayer graphene with a finite Coulomb interaction. However, it should be noted that our work is a different analysis, and our model can treat the temperature dependence self-consistently but is limited in the Mott regime, while their model can treat all of the filling factors but without a clear temperature dependence and is still awaiting self-consistent solutions.

ACKNOWLEDGMENTS

We would like to acknowledge very useful discussions with Y.-Z. Chou. This work was financially supported by the National Science Foundation Grants No. NSF-DMR-2002795 (Y.L. and M.D.) and No. NSF-DMR-2015639 (B.M.F.). Parts of this paper were written during the Aspen Center of Physics 2023 summer program on "New Directions on Strange Metals in Correlated Systems" (M.D.), which was supported by National Science Foundation Grant No. PHY-2210452.

[1] Y. Cao, V. Fatemi, A. Demir, S. Fang, S. L. Tomarken, J. Y. Luo, J. D. Sanchez-Yamagishi, K. Watanabe, T. Taniguchi, E. Kaxiras, R. C. Ashoori, and P. Jarillo-Herrero, Correlated insulator behaviour at half-filling in magic-angle graphene superlattices, Nature (London) **556**, 80 (2018).

[2] Y. Cao, V. Fatemi, S. Fang, K. Watanabe, T. Taniguchi, E. Kaxiras, and P. Jarillo-Herrero, Unconventional superconductivity in magic-angle graphene superlattices, Nature (London) **556**, 43 (2018).

[3] M. Yankowitz, S. Chen, H. Polshyn, Y. Zhang, K. Watanabe, T. Taniguchi, D. Graf, A. F. Young, and C. R. Dean, Tuning superconductivity in twisted bilayer graphene, Science **363**, 1059 (2019).

[4] A. L. Sharpe, E. J. Fox, A. W. Barnard, J. Finney, K. Watanabe, T. Taniguchi, M. A. Kastner, and D. Goldhaber-Gordon, Emergent ferromagnetism near three-quarters filling in twisted bilayer graphene, Science **365**, 605 (2019).

[5] M. Fleischmann, R. Gupta, F. Wullschläger, S. Theil, D. Weckbecker, V. Meded, S. Sharma, B. Meyer, and S. Shallcross, Perfect and controllable nesting in minimally twisted bilayer graphene, Nano Lett. **20**, 971 (2020).

[6] A. J. H. Jones, R. Muzzio, P. Majchrzak, S. Pakdel, D. Curcio, K. Volckaert, D. Biswas, J. Gobbo, S. Singh, J. T. Robinson, K. Watanabe, T. Taniguchi, T. K. Kim, C. Cacho, N. Lanata, J. A. Miwa, P. Hofmann, J. Katoch, and S. Ulstrup, Observation of electrically tunable van Hove singularities in twisted bilayer graphene from nanoARPES, Adv. Mater. **32**, 2001656 (2020).

[7] Y. Cao, J. M. Park, K. Watanabe, T. Taniguchi, and P. Jarillo-Herrero, Large Pauli limit violation and reentrant superconductivity in magic-angle twisted trilayer graphene, arXiv:2103.12083.

[8] S. Xu, M. M. Al Ezzi, N. Balakrishnan, A. Garcia-Ruiz, B. Tsim, C. Mullan, J. Barrier, N. Xin, B. A. Piot, T. Taniguchi, K. Watanabe, A. Carvalho, A. Mishchenko, A. K. Geim, V. I. Fal'ko, S. Adam, A. H. C. Neto, K. S. Novoselov, and Y. Shi, Tunable van Hove singularities and correlated states in twisted monolayer–bilayer graphene, Nat. Phys. **17**, 619 (2021).

[9] Y. Choi, H. Kim, Y. Peng, A. Thomson, C. Lewandowski, R. Polski, Y. Zhang, H. S. Arora, K. Watanabe, T. Taniguchi, J. Alicea, and S. Nadj-Perge, Correlation-driven topological phases in magic-angle twisted bilayer graphene, Nature (London) **589**, 536 (2021).

[10] J. M. Park, Y. Cao, L.-Q. Xia, S. Sun, K. Watanabe, T. Taniguchi, and P. Jarillo-Herrero, Robust superconductivity in magic-angle multilayer graphene family, Nat. Mater. **21**, 877 (2022).

[11] A. Uri, S. C. de la Barrera, M. T. Randeria, D. Rodan-Legrain, T. Devakul, P. J. D. Crowley, N. Paul, K. Watanabe, T. Taniguchi, R. Lifshitz, L. Fu, R. C. Ashoori, and P. Jarillo-Herrero, Superconductivity and strong interactions in a tunable moiré quasiperiodic crystal, arXiv:2302.00686.

[12] M. H. Naik and M. Jain, Ultraflatbands and shear solitons in moiré patterns of twisted bilayer transition metal dichalcogenides, Phys. Rev. Lett. **121**, 266401 (2018).

[13] Y. Tang, L. Li, T. Li, Y. Xu, S. Liu, K. Barmak, K. Watanabe, T. Taniguchi, A. H. MacDonald, J. Shan, and K. F. Mak, Simulation of Hubbard model physics in WSe_2/WS_2 moiré superlattices, Nature (London) **579**, 353 (2020).

[14] L. Wang, E.-M. Shih, A. Ghiotto, L. Xian, D. A. Rhodes, C. Tan, M. Claassen, D. M. Kennes, Y. Bai, B. Kim, K. Watanabe, T. Taniguchi, X. Zhu, J. Hone, A. Rubio, A. N. Pasupathy, and C. R. Dean, Correlated electronic phases in twisted bilayer transition metal dichalcogenides, Nat. Mater. **19**, 861 (2020).

[15] L. Zhang, Z. Zhang, F. Wu, D. Wang, R. Gogna, S. Hou, K. Watanabe, T. Taniguchi, K. Kulkarni, T. Kuo, S. R. Forrest, and H. Deng, Twist-angle dependence of moiré excitons in $WS_2/MoSe_2$ heterobilayers, Nat. Commun. **11**, 5888 (2020).

[16] S. Shabani, D. Halbertal, W. Wu, M. Chen, S. Liu, J. Hone, W. Yao, D. N. Basov, X. Zhu, and A. N. Pasupathy, Deep moiré potentials in twisted transition metal dichalcogenide bilayers, Nat. Phys. **17**, 720 (2021).

[17] Y. Xu, K. Kang, K. Watanabe, T. Taniguchi, K. F. Mak, and J. Shan, A tunable bilayer Hubbard model in twisted WSe_2, Nat. Nanotechnol. **17**, 934 (2022).

[18] Y. Xiong, Y. Wang, R. Zhu, H. Xu, C. Wu, J. Chen, Y. Ma, Y. Liu, Y. Chen, K. Watanabe, T. Taniguchi, M. Shi, X. Chen, Y. Lu, P. Zhan, Y. Hao, and F. Xu, Twisted black phosphorus-based van der Waals stacks for fiber-integrated polarimeters, Sci. Adv. **8**, eabo0375 (2022).

[19] Z. Meng, L. Wang, W. Han, F. Liu, K. Wen, C. Gao, P. Wang, C. Chin, and J. Zhang, Atomic Bose–Einstein condensate in twisted-bilayer optical lattices, Nature (London) **615**, 231 (2023).

[20] D. M. Kennes, M. Claassen, L. Xian, A. Georges, A. J. Millis, J. Hone, C. R. Dean, D. N. Basov, A. N. Pasupathy, and A. Rubio, Moiré heterostructures as a condensed-matter quantum simulator, Nat. Phys. **17**, 155 (2021).

[21] C. Xu and L. Balents, Topological superconductivity in twisted multilayer graphene, Phys. Rev. Lett. **121**, 087001 (2018).

[22] H. C. Po, L. Zou, A. Vishwanath, and T. Senthil, Origin of Mott insulating behavior and superconductivity in twisted bilayer graphene, Phys. Rev. X **8**, 031089 (2018).

[23] F. Wu, T. Lovorn, E. Tutuc, and A. H. MacDonald, Hubbard model physics in transition metal dichalcogenide moiré bands, Phys. Rev. Lett. **121**, 026402 (2018).

[24] J. Kang and O. Vafek, Symmetry, maximally localized Wannier states, and a low-energy model for twisted bilayer graphene narrow bands, Phys. Rev. X **8**, 031088 (2018).

[25] J. Kang and O. Vafek, Strong coupling phases of partially filled twisted bilayer graphene narrow bands, Phys. Rev. Lett. **122**, 246401 (2019).

[26] K. Seo, V. N. Kotov, and B. Uchoa, Ferromagnetic Mott state in twisted graphene bilayers at the magic angle, Phys. Rev. Lett. **122**, 246402 (2019).

[27] M. Koshino, Band structure and topological properties of twisted double bilayer graphene, Phys. Rev. B **99**, 235406 (2019).

[28] K. Hejazi, C. Liu, H. Shapourian, X. Chen, and L. Balents, Multiple topological transitions in twisted bilayer graphene near the first magic angle, Phys. Rev. B **99**, 035111 (2019).

[29] N. R. Chebrolu, B. L. Chittari, and J. Jung, Flat bands in twisted double bilayer graphene, Phys. Rev. B **99**, 235417 (2019).

[30] T. Cea, N. R. Walet, and F. Guinea, Electronic band structure and pinning of fermi energy to Van Hove singularities in twisted bilayer graphene: A self-consistent approach, Phys. Rev. B **100**, 205113 (2019).

[31] J. Liu, Z. Ma, J. Gao, and X. Dai, Quantum valley Hall effect, orbital magnetism, and anomalous Hall effect in twisted multilayer graphene systems, Phys. Rev. X **9**, 031021 (2019).

[32] X. Liang, Z. A. H. Goodwin, V. Vitale, F. Corsetti, A. A. Mostofi, and J. Lischner, Effect of bilayer stacking on the atomic and electronic structure of twisted double bilayer graphene, Phys. Rev. B **102**, 155146 (2020).

[33] K. Tran, J. Choi, and A. Singh, Moiré and beyond in transition metal dichalcogenide twisted bilayers, 2D Mater. **8**, 022002 (2021).
[34] G. A. Tritsaris, S. Carr, Z. Zhu, Y. Xie, S. B. Torrisi, J. Tang, M. Mattheakis, D. T. Larson, and E. Kaxiras, Electronic structure calculations of twisted multi-layer graphene superlattices, 2D Mater. **7**, 035028 (2020).
[35] E. Lake and T. Senthil, Reentrant superconductivity through a quantum Lifshitz transition in twisted trilayer graphene, Phys. Rev. B **104**, 174505 (2021).
[36] W. Qin and A. H. MacDonald, In-plane critical magnetic fields in magic-angle twisted trilayer graphene, Phys. Rev. Lett. **127**, 097001 (2021).
[37] A. Eaton, Y. Li, H. A. Fertig, and B. Seradjeh, Renormalized magic angles in asymmetric twisted graphene multilayers, Phys. Rev. B **106**, 045117 (2022).
[38] Y. Zhou, D. N. Sheng, and E.-A. Kim, Quantum phases of transition metal dichalcogenide moiré systems, Phys. Rev. Lett. **128**, 157602 (2022).
[39] C. Valagiannopoulos, Electromagnetic analog to magic angles in twisted bilayers of two-dimensional media, Phys. Rev. Appl. **18**, 044011 (2022).
[40] K. Adhikari, K. Seo, K. S. D. Beach, and B. Uchoa, Strongly interacting phases in twisted bilayer graphene at the magic angle, arXiv:2308.03843.
[41] G. E. Topp, G. Jotzu, J. W. McIver, L. Xian, A. Rubio, and M. A. Sentef, Topological Floquet engineering of twisted bilayer graphene, Phys. Rev. Res. **1**, 023031 (2019).
[42] Y. Li, H. A. Fertig, and B. Seradjeh, Floquet-engineered topological flat bands in irradiated twisted bilayer graphene, Phys. Rev. Res. **2**, 043275 (2020).
[43] O. Katz, G. Refael, and N. H. Lindner, Optically induced flat bands in twisted bilayer graphene, Phys. Rev. B **102**, 155123 (2020).
[44] M. Vogl, M. Rodriguez-Vega, and G. A. Fiete, Effective Floquet Hamiltonians for periodically driven twisted bilayer graphene, Phys. Rev. B **101**, 235411 (2020).
[45] M. Vogl, M. Rodriguez-Vega, B. Flebus, A. H. MacDonald, and G. A. Fiete, Floquet engineering of topological transitions in a twisted transition metal dichalcogenide homobilayer, Phys. Rev. B **103**, 014310 (2021).
[46] R. Bistritzer and A. H. MacDonald, Moiré bands in twisted double-layer graphene, Proc. Natl. Acad. Sci. USA **108**, 12233 (2011).
[47] J. M. B. Lopes dos Santos, N. M. R. Peres, and A. H. Castro Neto, Graphene bilayer with a twist: Electronic structure, Phys. Rev. Lett. **99**, 256802 (2007).
[48] S. Shallcross, S. Sharma, and O. A. Pankratov, Quantum interference at the twist boundary in graphene, Phys. Rev. Lett. **101**, 056803 (2008).
[49] S. Shallcross, S. Sharma, E. Kandelaki, and O. A. Pankratov, Electronic structure of turbostratic graphene, Phys. Rev. B **81**, 165105 (2010).
[50] E. J. Mele, Commensuration and interlayer coherence in twisted bilayer graphene, Phys. Rev. B **81**, 161405(R) (2010).
[51] E. J. Mele, Band symmetries and singularities in twisted multilayer graphene, Phys. Rev. B **84**, 235439 (2011).
[52] S. Carr, D. Massatt, S. Fang, P. Cazeaux, M. Luskin, and E. Kaxiras, Twistronics: Manipulating the electronic properties of two-dimensional layered structures through their twist angle, Phys. Rev. B **95**, 075420 (2017).
[53] G. Tarnopolsky, A. J. Kruchkov, and A. Vishwanath, Origin of magic angles in twisted bilayer graphene, Phys. Rev. Lett. **122**, 106405 (2019).
[54] E. Khalaf, A. J. Kruchkov, G. Tarnopolsky, and A. Vishwanath, Magic angle hierarchy in twisted graphene multilayers, Phys. Rev. B **100**, 085109 (2019).
[55] Y. Li, A. Eaton, H. A. Fertig, and B. Seradjeh, Dirac magic and Lifshitz transitions in AA-stacked twisted multilayer graphene, Phys. Rev. Lett. **128**, 026404 (2022).
[56] Y. Cao, D. Chowdhury, D. Rodan-Legrain, O. Rubies-Bigorda, K. Watanabe, T. Taniguchi, T. Senthil, and P. Jarillo-Herrero, Strange metal in magic-angle graphene with near Planckian dissipation, Phys. Rev. Lett. **124**, 076801 (2020).
[57] F. Wu, A. H. MacDonald, and I. Martin, Theory of phonon-mediated superconductivity in twisted bilayer graphene, Phys. Rev. Lett. **121**, 257001 (2018).
[58] B. Lian, Z. Wang, and B. A. Bernevig, Twisted bilayer graphene: A phonon-driven superconductor, Phys. Rev. Lett. **122**, 257002 (2019).
[59] J. González and T. Stauber, Kohn-Luttinger superconductivity in twisted bilayer graphene, Phys. Rev. Lett. **122**, 026801 (2019).
[60] M. Christos, S. Sachdev, and M. S. Scheurer, Correlated insulators, semimetals, and superconductivity in twisted trilayer graphene, Phys. Rev. X **12**, 021018 (2022).
[61] A. Fischer, Z. A. H. Goodwin, A. A. Mostofi, J. Lischner, D. M. Kennes, and L. Klebl, Unconventional superconductivity in magic-angle twisted trilayer graphene, npj Quantum Mater. **7**, 5 (2022).
[62] J. Liu, J. Liu, and X. Dai, Pseudo Landau level representation of twisted bilayer graphene: Band topology and implications on the correlated insulating phase, Phys. Rev. B **99**, 155415 (2019).
[63] M. J. Calderón and E. Bascones, Interactions in the 8-orbital model for twisted bilayer graphene, Phys. Rev. B **102**, 155149 (2020).
[64] A. Ramires and J. L. Lado, Emulating heavy fermions in twisted trilayer graphene, Phys. Rev. Lett. **127**, 026401 (2021).
[65] Z.-D. Song and B. A. Bernevig, Magic-angle twisted bilayer graphene as a topological heavy fermion problem, Phys. Rev. Lett. **129**, 047601 (2022).
[66] Y. Xie, B. Lian, B. Jäck, X. Liu, C.-L. Chiu, K. Watanabe, T. Taniguchi, B. A. Bernevig, and A. Yazdani, Spectroscopic signatures of many-body correlations in magic-angle twisted bilayer graphene, Nature (London) **572**, 101 (2019).
[67] D. Wong, K. P. Nuckolls, M. Oh, B. Lian, Y. Xie, S. Jeon, K. Watanabe, T. Taniguchi, B. A. Bernevig, and A. Yazdani, Cascade of electronic transitions in magic-angle twisted bilayer graphene, Nature (London) **582**, 198 (2020).
[68] N. Tilak, X. Lai, S. Wu, Z. Zhang, M. Xu, R. d. A. Ribeiro, P. C. Canfield, and E. Y. Andrei, Flat band carrier confinement in magic-angle twisted bilayer graphene, Nat. Commun. **12**, 4180 (2021).
[69] H. Shi and X. Dai, Heavy-fermion representation for twisted bilayer graphene systems, Phys. Rev. B **106**, 245129 (2022).
[70] Y.-Z. Chou and S. Das Sarma, Kondo lattice model in magic-angle twisted bilayer graphene, Phys. Rev. Lett. **131**, 026501 (2023).

[71] J. Yu, M. Xie, B. A. Bernevig, and S. Das Sarma, Magic-angle twisted symmetric trilayer graphene as a topological heavy-fermion problem, Phys. Rev. B **108**, 035129 (2023).

[72] H. Hu, G. Rai, L. Crippa, J. Herzog-Arbeitman, D. Călugăru, T. Wehling, G. Sangiovanni, R. Valentí, A. M. Tsvelik, and B. A. Bernevig, Symmetric Kondo lattice states in doped strained twisted bilayer graphene, Phys. Rev. Lett. **131**, 166501 (2023).

[73] H. Hu, B. A. Bernevig, and A. M. Tsvelik, Kondo lattice model of magic-angle twisted-bilayer graphene: Hund's rule, local-moment fluctuations, and low-energy effective theory, Phys. Rev. Lett. **131**, 026502 (2023).

[74] G.-D. Zhou, Y.-J. Wang, N. Tong, and Z.-D. Song, Kondo phase in twisted bilayer graphene, Phys. Rev. B **109**, 045419 (2024).

[75] A. Datta, M. J. Calderón, A. Camjayi, and E. Bascones, Heavy quasiparticles and cascades without symmetry breaking in twisted bilayer graphene, Nat. Commun. **14**, 5036 (2023).

[76] C. Huang, X. Zhang, G. Pan, H. Li, K. Sun, X. Dai, and Z. Y. Meng, Evolution from quantum anomalous Hall insulator to heavy-fermion semimetal in magic-angle twisted bilayer graphene, Phys. Rev. B **109**, 125404 (2024).

[77] D. Călugăru, M. Borovkov, L. L. H. Lau, P. Coleman, Z.-D. Song, and B. A. Bernevig, Twisted bilayer graphene as topological heavy fermion: II. Analytical approximations of the model parameters, Low Temp. Phys. **49**, 640 (2023).

[78] K. Singh, A. Chew, J. Herzog-Arbeitman, B. A. Bernevig, and O. Vafek, Topological heavy fermions in magnetic field, Nat. Commun. **15**, 5257 (2024).

[79] Y.-Z. Chou and S. Das Sarma, Scaling theory of intrinsic Kondo and Hund's rule interactions in magic-angle twisted bilayer graphene, Phys. Rev. B **108**, 125106 (2023).

[80] A. Rozen, J. M. Park, U. Zondiner, Y. Cao, D. Rodan-Legrain, T. Taniguchi, K. Watanabe, Y. Oreg, A. Stern, E. Berg, P. Jarillo-Herrero, and S. Ilani, Entropic evidence for a Pomeranchuk effect in magic-angle graphene, Nature (London) **592**, 214 (2021).

[81] Y. Saito, F. Yang, J. Ge, X. Liu, T. Taniguchi, K. Watanabe, J. I. A. Li, E. Berg, and A. F. Young, Isospin Pomeranchuk effect in twisted bilayer graphene, Nature (London) **592**, 220 (2021).

[82] U. Zondiner, A. Rozen, D. Rodan-Legrain, Y. Cao, R. Queiroz, T. Taniguchi, K. Watanabe, Y. Oreg, F. von Oppen, A. Stern, E. Berg, P. Jarillo-Herrero, and S. Ilani, Cascade of phase transitions and Dirac revivals in magic-angle graphene, Nature (London) **582**, 203 (2020).

[83] M. Oh, K. P. Nuckolls, D. Wong, R. L. Lee, X. Liu, K. Watanabe, T. Taniguchi, and A. Yazdani, Evidence for unconventional superconductivity in twisted bilayer graphene, Nature (London) **600**, 240 (2021).

[84] M. Lavagna, A. J. Millis, and P. A. Lee, d-wave superconductivity in the large-degeneracy limit of the Anderson lattice, Phys. Rev. Lett. **58**, 266 (1987).

[85] See Supplemental Material at http://link.aps.org/supplemental/10.1103/PhysRevB.110.045123 for the detailed derivation of the mean-field equations.

[86] M. O. Dzero, L. P. Gor'kov, and A. K. Zvezdin, First-order valence transition in $YbInCu_4$ in the (B, T)-plane, J. Phys.: Condens. Matter **12**, L711 (2000).

[87] J.-T. Zhuang, X.-J. Zheng, Z.-Y. Wang, X. Ming, H. Li, Y. Liu, and H.-F. Song, Valence transition in topological Kondo insulator, J. Phys.: Condens. Matter **32**, 035602 (2020).

[88] K. Kummer, C. Geibel, C. Krellner, G. Zwicknagl, C. Laubschat, N. B. Brookes, and D. V. Vyalikh, Similar temperature scale for valence changes in Kondo lattices with different Kondo temperatures, Nat. Commun. **9**, 2011 (2018).

[89] F. Frontini, B. W. Lebert, K. K. Cho, M. S. Song, B. K. Cho, C. J. Pollock, and Y.-J. Kim, Intermediate valence state in YbB_4 revealed by resonant x-ray emission spectroscopy, J. Phys.: Condens. Matter **34**, 345601 (2022).

[90] S. R. Panday and M. Dzero, Superconductivity in Ce-based cage compounds, J. Phys.: Condens. Matter **35**, 335601 (2023).

[91] Y. Onishi and K. Miyake, Enhanced valence fluctuations caused by f-c Coulomb interaction in Ce-based heavy electrons: Possible origin of pressure-induced enhancement of superconducting transition temperature in $CeCu_2Ge_2$ and related compounds, J. Phys. Soc. Jpn. **69**, 3955 (2000).

[92] L. L. H. Lau and P. Coleman, Topological mixed valence model for twisted bilayer graphene, arXiv:2303.02670.